HEDL-SA-1867 FP
CONF-791103--49

COMPUTATIONAL BENCHMARK FOR DEEP PENETRATION IN IRON

L. L. Carter and J. S. Hendricks*

October 1979

American Nuclear Society

November 12-15, 1979

San Francisco, California

HANFORD ENGINEERING DEVELOPMENT LABORATORY
Operated by Westinghouse Hanford Company, a subsidiary of Westinghouse Electric Corporation, under the Department of Energy Contract No. DE-AC14-76FF02170

*Los Alamos Scientific Laboratory

DISCLAIMER

COMPUTATIONAL BENCHMARK FOR DEEP PENETRATION IN IRON

L. L. Carter and J. S. Hendricks

Neutron transport through thick regions of iron is important in many fast reactor and fusion applications. The resonance structure of the iron cross sections from 20 keV to about 2 MeV introduces considerable complexity into calculations of the transport. To compound the problem the shield designer may be under severe time constraints including the use of computer codes and cross section sets with which he is not intimately familiar.

Ideally, comparisons should be made between relevant experimental measurements and calculations (using the same cross section sets and transport codes that will be used in design studies) before making the calculations for the shield design. Even if there is time to do this, the relevant experimental measurements often introduce two- or three-dimensional effects requiring computer codes for the analysis that would not otherwise be needed.

Consider, for example, a measurement of neutron penetration through iron slabs made at Oak Ridge National Laboratory. The geometry shown on slide #1 is relatively simple, but does require a two-dimensional calculation for a good analysis. The resonance structure of the iron cross sections makes it highly desirable to utilize a two-dimensional Monte Carlo calculation with a pointwise treatment of the cross sections. Such an analysis has been done by Guy Estes and John Hendricks and will be

summarized in the first paper in the "Nuclear Data for Shielding Applications" session tomorrow afternoon. The time required to do this type of analysis confirms the need for a simpler calculational benchmark.

In this paper we are describing a benchmark calculation of neutron transport through a thick slab of iron. The calculation utilizes the same Monte Carlo code (MCNP) along with the ENDF/B-IV and V based cross section sets that were used to make comparisons with the Oak Ridge experiment. This one-dimensional calculational benchmark has been documented in a Los Alamos Scientific Laboratory report.

The geometry for the benchmark problem is shown on slide #2. Monoenergetic neutron sources of 2, 14, and 40 MeV are normally incident upon a three meter thick iron slab. The resulting neutron currents, flux, and radiation dose are tabulated in a standard energy group structure at various distances through the slab.

The principal advantage of the MCNP Monte Carlo code for this application is that the multigroup approximation is not required and hence resonance self-shielding is accounted for automatically. The only significant difference between the cross section data in the MCNP library and the ENDF/B data base from which it is derived via the NJOY processing code is that resonance data are represented in MCNP as linearly interpolated pointwise data Doppler broadened to a specific temperature. This representation is shown on slide #3 for the ENDF/B-IV total cross section of iron between 10 keV and about 300 keV. Over 1300 energy points were used to describe the cross section within this energy interval.

We will now display some figures summarizing the benchmark calculations. The benchmark not only provides tabulated data for confirming the accuracy of multigroup calculations, but it also provides the necessary numerical data for obtaining insights into the spectral and spatial distribution of the neutrons as they penetrate into iron.

The spatial distribution of the total flux is shown on slide #4 for the three monoenergetic sources. Cross sections based upon both ENDF/B-IV and ENDF/B-V were used for the 2 and 14 MeV sources. The library based upon ENDF/B-IV was extended above 20 MeV for the calculations with the 40 MeV source.

Focusing upon the 14 MeV source curves, we observe that the total flux calculated from the two data bases is in good agreement out to about one meter. Beyond one meter the curves diverge until at 2.5 meters the total flux calculated with the ENDF/B-V data is about a factor of two greater than that obtained from the ENDF/B-IV data. Similar results are obtained for the 2 MeV source.

We also note that the total flux within the slab increases as the energy of the incident neutron is increased. This is apparently due to two effects: (1) A higher energy neutron penetrates further into the slab before significant moderation occurs and this decreases the probability of leakage back out of the source face. (2) The higher energy neutrons produce additional neutrons from (n,2n) reactions.

Curves are shown on slide #5 for the radiation dose through the slab for the same sources and cross section sets.

The energy dependent flux, calculated with the ENDF/B-V data, is shown on slide #6 at one meter into the slab for the 2 and 14 MeV sources. The flux due to the 2 MeV source is uniformly lower than that due to the 14 MeV source for energies less than 500 keV. Above 500 keV some changes occur due to the proximity to the 2 MeV monoenergetic source energy.

Spectral comparisons are similar at two meters into the slab as shown on slide #7.

There is a gradual downward shift in neutron energy with penetration distance into the slab as shown on slide #8 for the 14 MeV source. Most of the neutrons suffer inelastic collisions within the first few centimeters of penetration which degrades their energy below the lowest inelastic threshold. Then the spectral shift is entirely by elastic scattering with the heavy iron nuclei.

The percentage difference between spectra calculated with ENDF/B-IV and ENDF/B-V data are shown on slide #9 at a penetration distance of one meter. There is a definite change in the sign of the difference at about 500 keV. These percentage differences increase with penetration distance into the slab.

The percentage difference is shown on slide #10 at a penetration distance of two meters. Some of the points on these last two slides are not valid comparison points due to the associated statistical errors. These have been set to zero and flagged with an arrow on the slides.

The one standard deviation relative statistical error is shown on slide #11 at two meters into the slab. These fluxes were generated with

multi-hour runs on the CDC-7600 computer and so have small statistical errors. Two computer runs were made for each source energy, one to generate the dominant flux profile and the other to optimize the calculation for obtaining the flux above 0.743 MeV. This explains the dramatic improvement in the statistical error at group 28. The dominant flux profile was calculated using importances that varied from unity at the source face to 4096 at maximum penetration, while the high energy component was calculated with an importance change of more than 10^9.

An example of the tabulated flux and dose data at one meter into the slab is given on slide #12 for the 2 MeV source. The tabulation is given for both ENDF/B-IV and ENDF/B-V data bases as a function of energy group. The PCNT. ERROR columns are the corresponding statistical errors expressed in percent for one standard deviation.

In summary, a calculational benchmark of neutron transport through iron is now available based upon a rigorous Monte Carlo treatment of ENDF/B-IV and ENDF/B-V cross sections. The currents, flux, and dose (from monoenergetic 2, 14, and 40 MeV sources) have been tabulated at various distances through the slab using a standard energy group structure. This tabulation is available in a Los Alamos Scientific Laboratory report.

The benchmark is simple to model and should be useful for verifying the adequacy of one-dimensional transport codes and multigroup libraries for iron. This benchmark also provides useful insights regarding neutron penetration through iron and displays differences in fluxes calculated with ENDF/B-IV and ENDF/B-V data bases. We are finding many uses for the benchmark and trust that others will also.

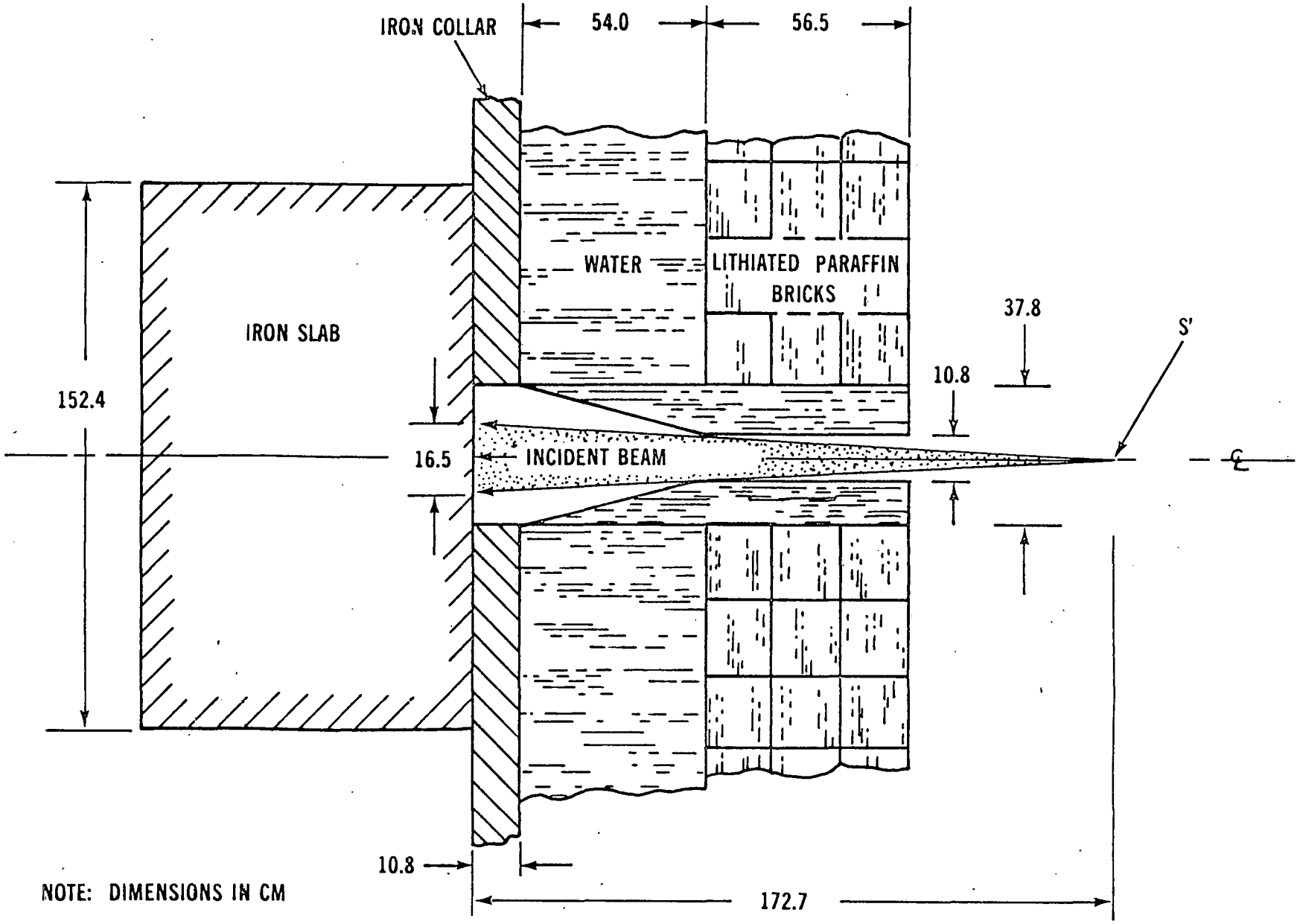

HEDL 7910-141.1

Slide 1

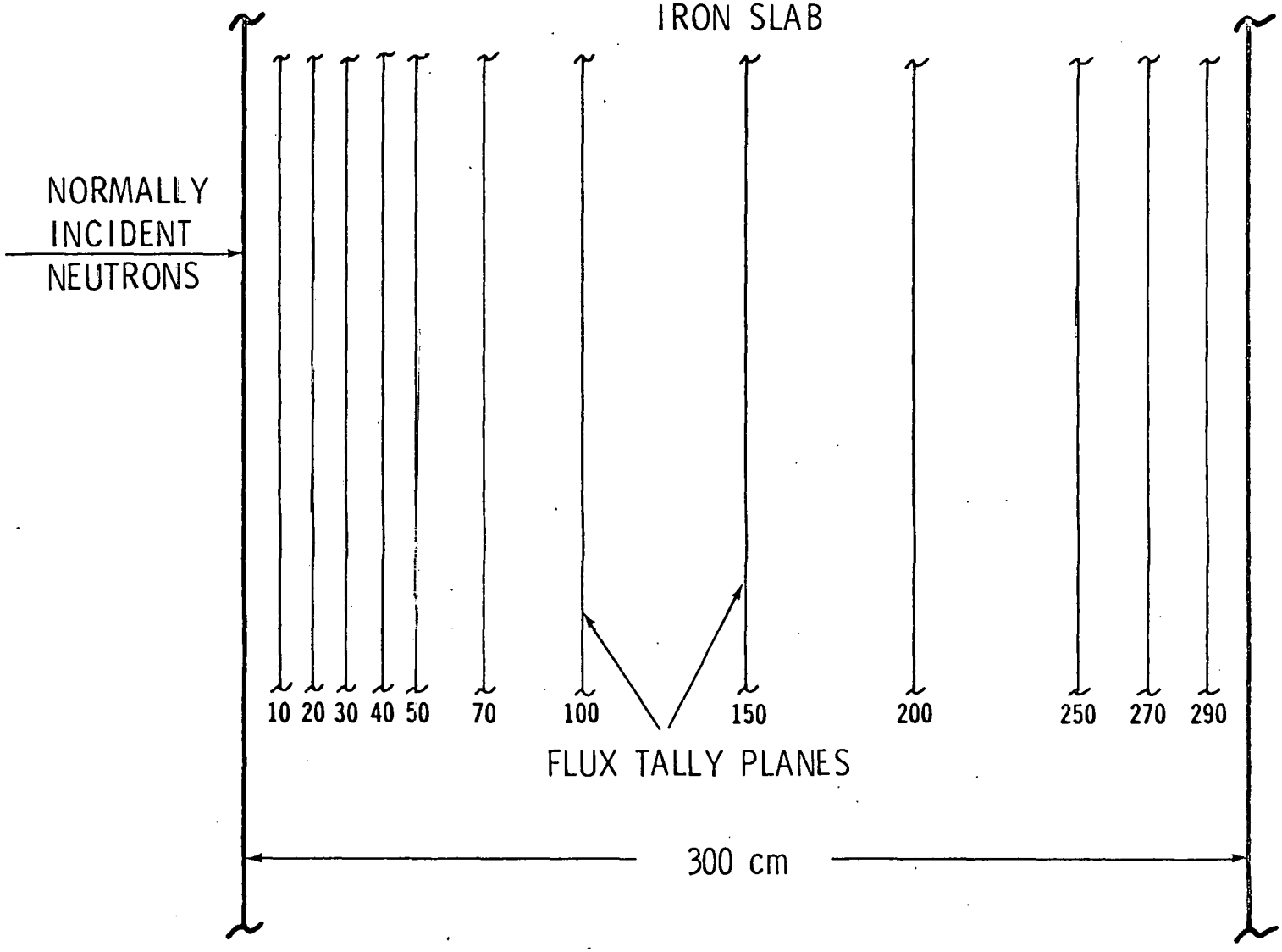

HEDL 7910-141.2

Slide 2

ENDF/B-4 TOTAL CROSS SECTION OF IRON

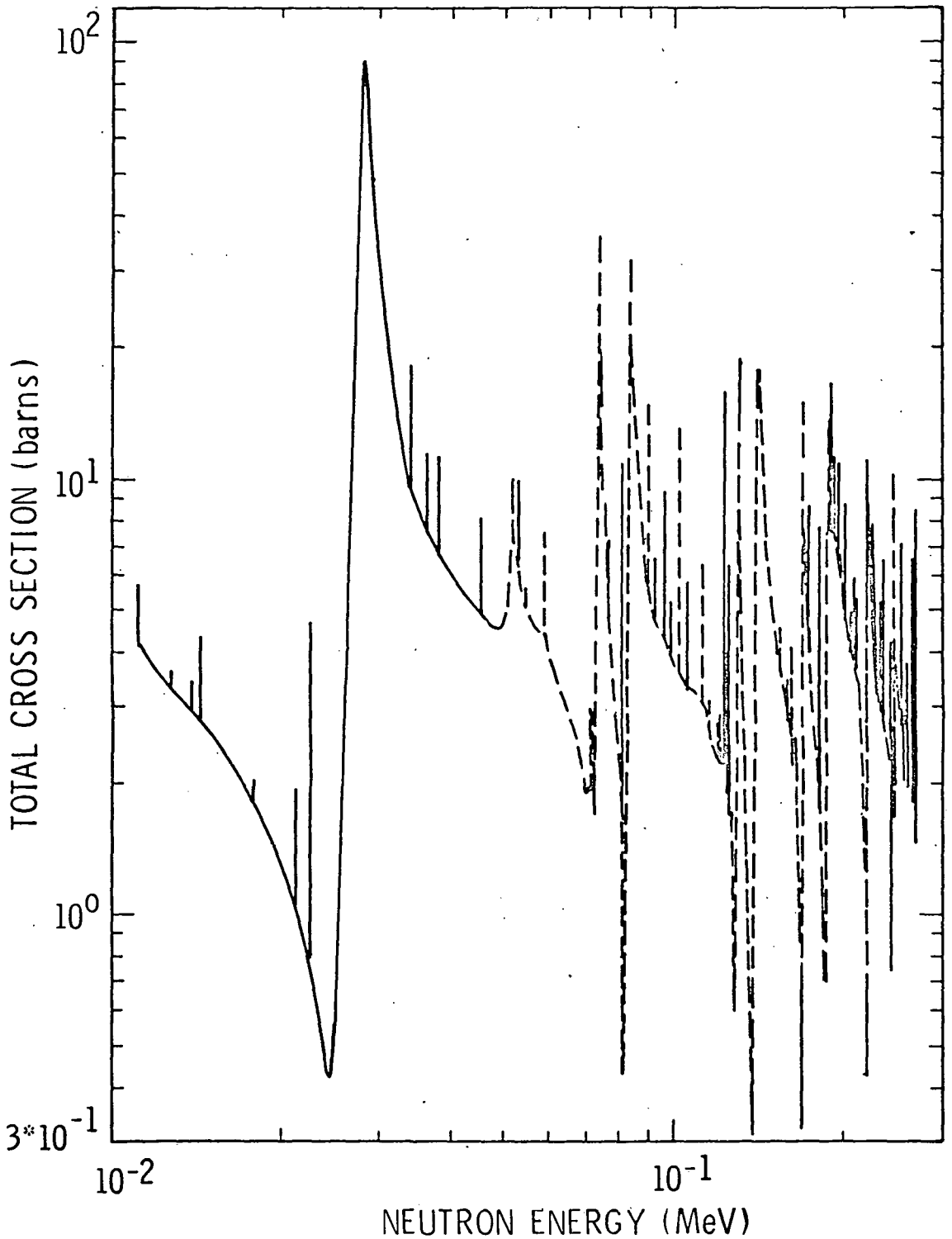

HEDL 7910-141.3

TOTAL NEUTRON FLUX WITHIN SLAB

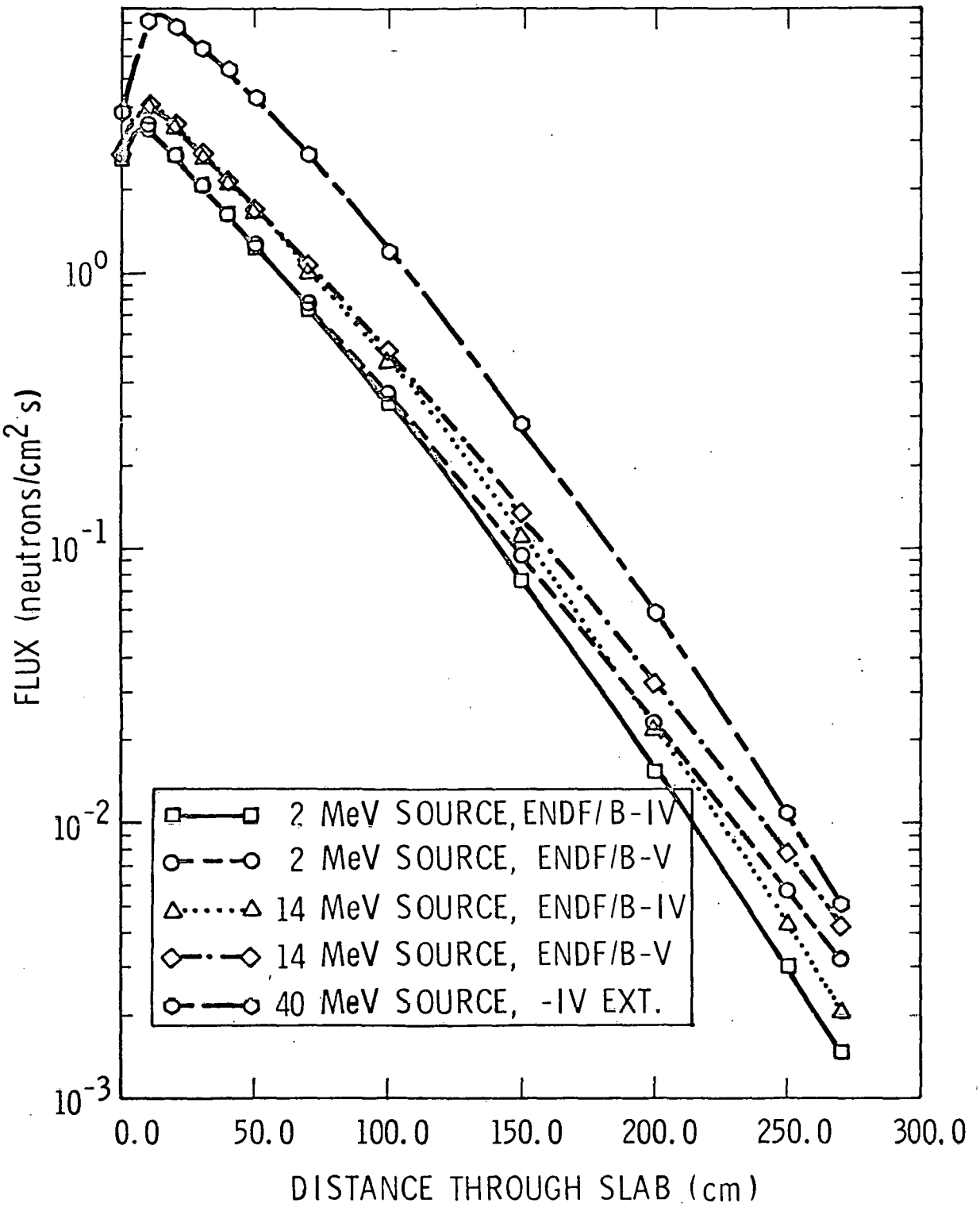

HEDL 7910-141.4

DOSE WITHIN SLAB

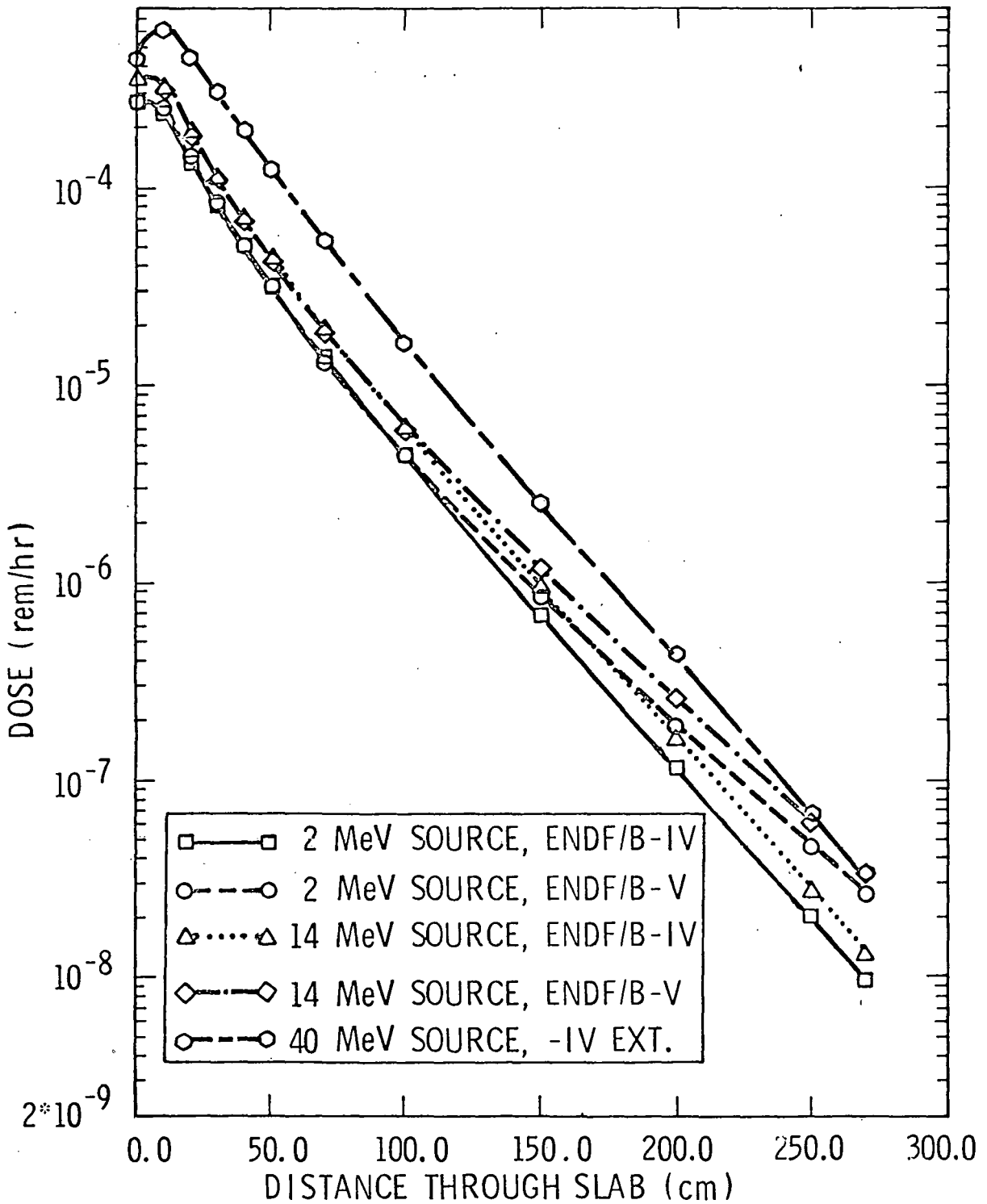

HEDL 7910-141.5

FLUX AT 100 CM INTO IRON SLAB

ENDF/B-5 CROSS SECTIONS

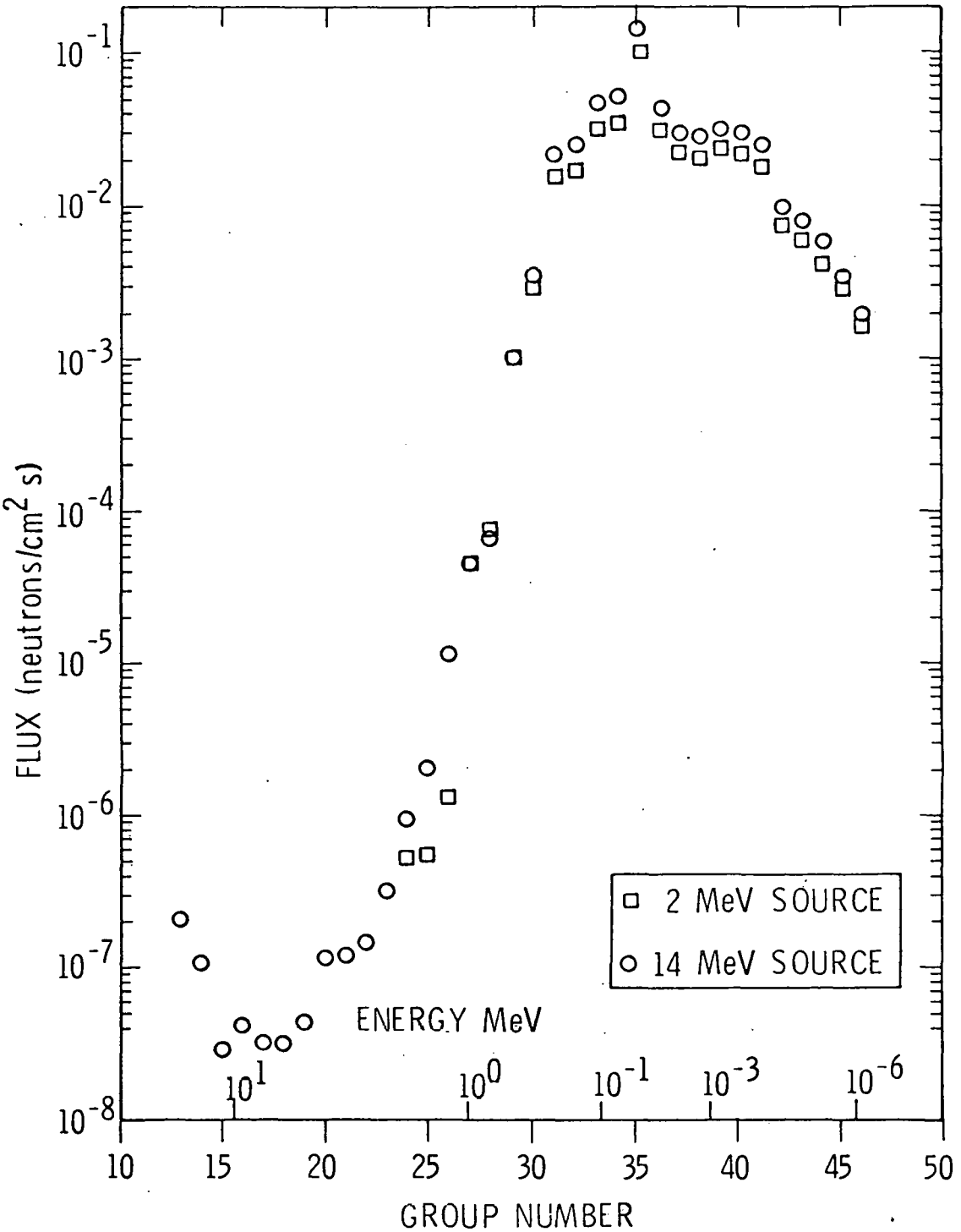

HEDL 7910-141.6

FLUX AT 200 CM INTO IRON SLAB

ENDF/B-5 CROSS SECTIONS

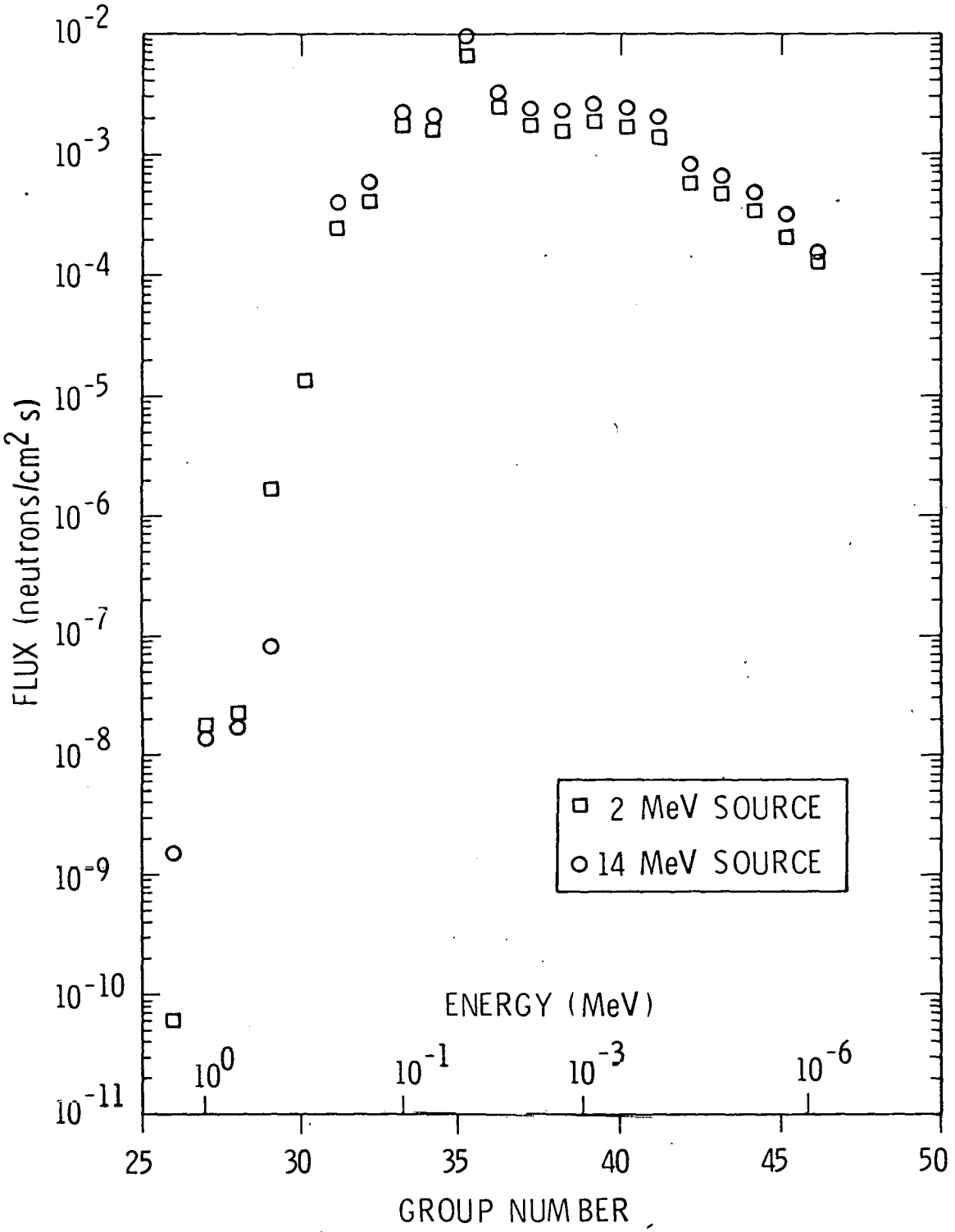

HEDL 7910-141.7

NORMALIZED FLUX SPECTRA

ENDF/B-5 CROSS SECTIONS

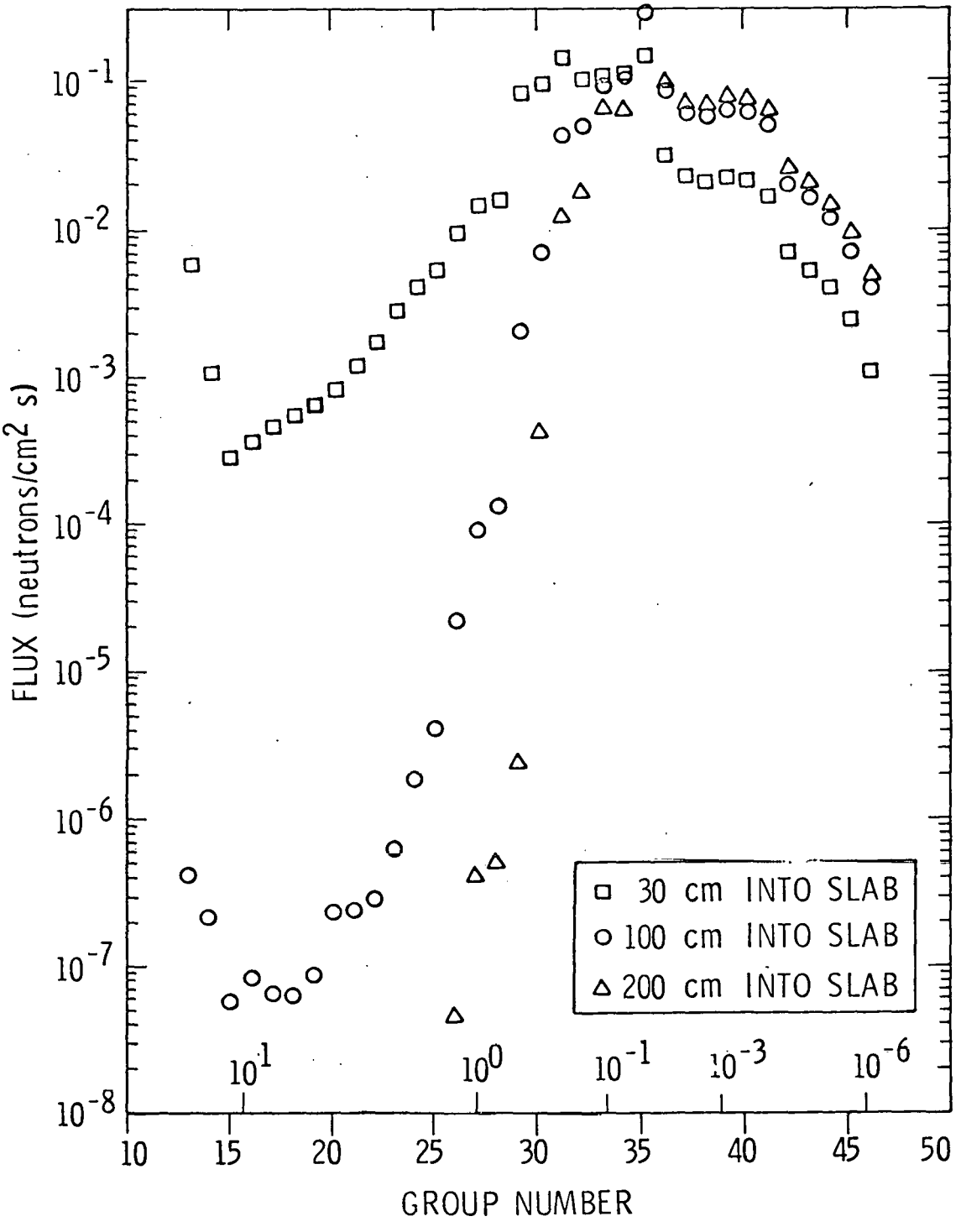

HEDL 7910-141.8

FLUX AT 100 CM INTO IRON SLAB

FLUX OF (v - iv / v) X 100

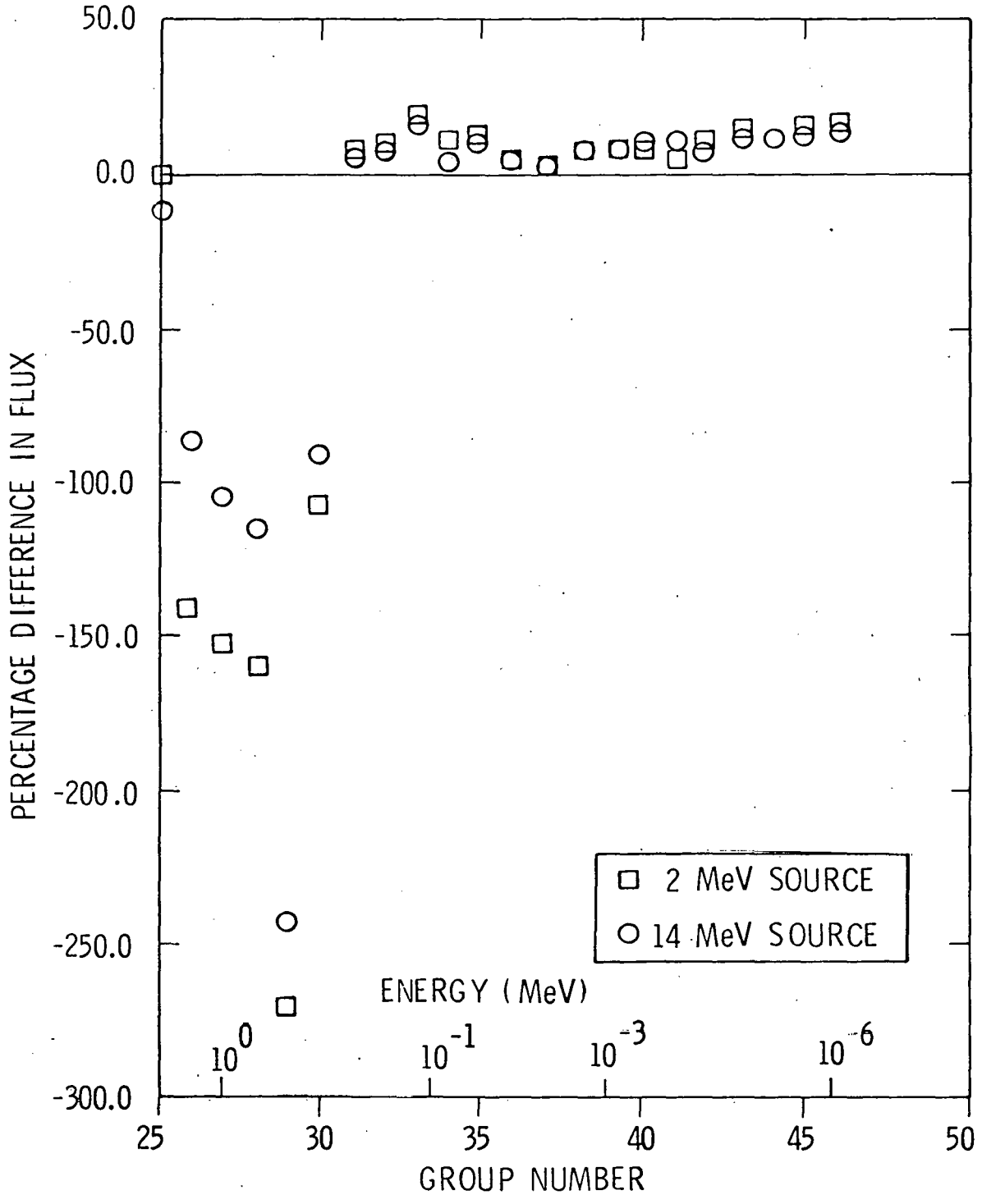

HEDL 7910-141.9

FLUX AT 200 CM INTO IRON SLAB

FLUX OF (v - iv / v) X 100

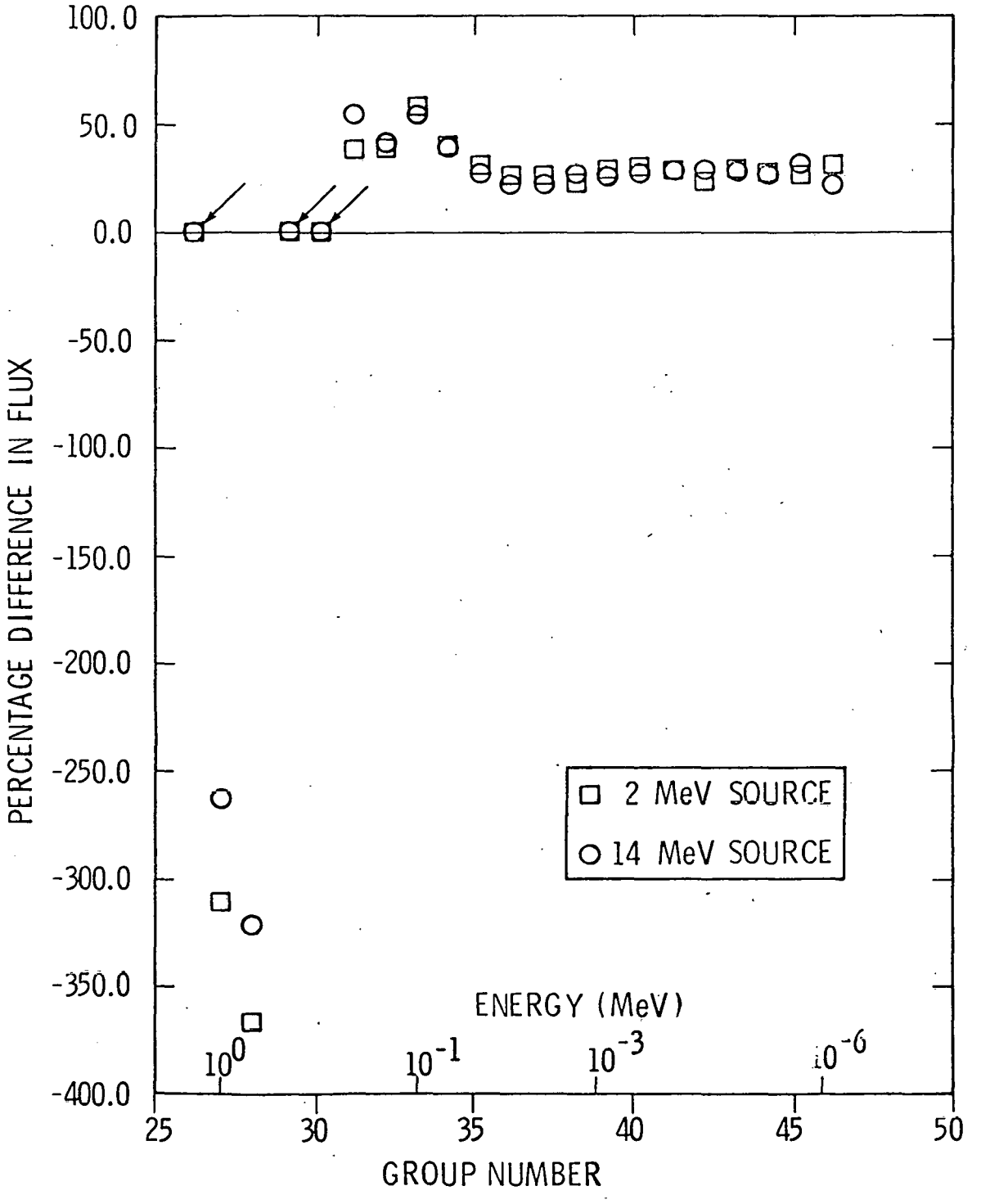

HEDL 7910-141.10

FLUX AT 200 CM INTO IRON SLAB

ENDF/B-5 CROSS SECTIONS

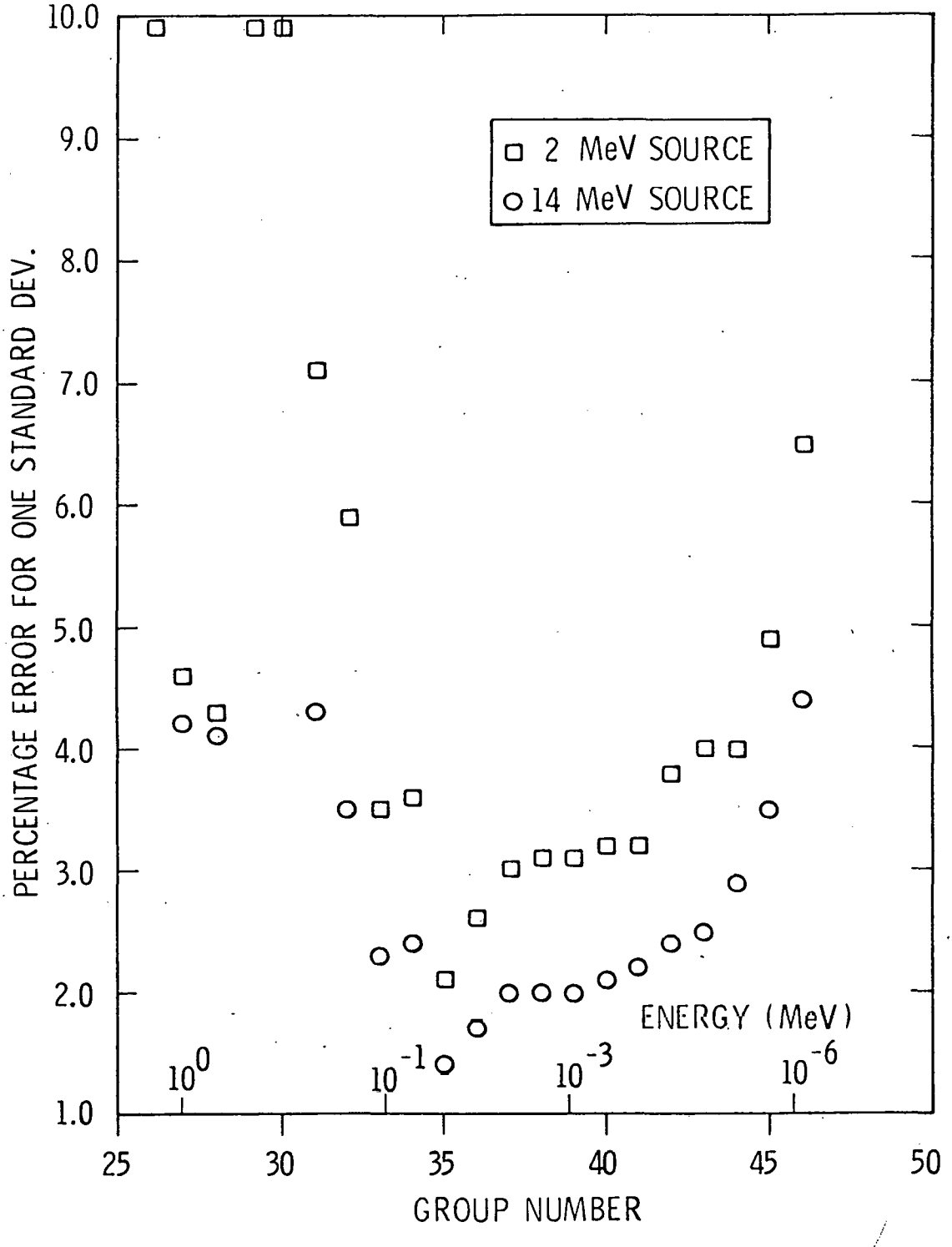

HEDL 7910-141.11

2-MeV SOURCE

SLAB THICKNESS = 100.0 cm

ENERGY (MeV)	******** FLUX ($N/cm^2/s$)	ENDF/B-IV PCNT. ERROR	******** DOSE (REM/HR)	PCNT. ERROR	******** FLUX ($N/cm^2/s$)	ENDF/B-V PCNT. ERROR	******** DOSE (REM/HR)	PCNT. ERROR
4.14E-07	3.5135E-04	13.9	1.3917E-09	13.9	3.9718E-04	15.9	1.5732E-09	15.9
1.12E-06	1.3558E-03	7.7	5.9491E-09	7.7	1.6073E-03	6.8	7.0528E-09	6.8
2.38E-06	2.4102E-03	5.4	1.0906E-08	5.4	2.8370E-03	5.6	1.2837E-08	5.6
5.04E-06	3.9039E-03	4.7	1.7856E-08	4.7	4.1363E-03	4.4	1.8919E-08	4.4
1.07E-05	5.1753E-03	4.0	2.3589E-08	4.0	6.0194E-03	4.0	2.7436E-08	4.0
2.26E-05	6.8306E-03	4.1	3.0670E-08	4.1	7.5614E-03	3.9	3.3951E-08	3.9
1.01E-04	1.7405E-02	3.3	7.5120E-08	3.3	1.8181E-02	3.4	7.8469E-08	3.4
4.54E-04	2.0054E-02	3.4	8.0859E-08	3.4	2.1779E-02	3.2	8.7811E-08	3.2
1.58E-03	2.1807E-02	3.2	8.2536E-08	3.2	2.3497E-02	3.1	8.8935E-08	3.1
3.35E-03	1.9030E-02	3.1	6.9382E-08	3.1	2.0471E-02	3.0	7.4636E-08	3.0
7.10E-03	2.2088E-02	3.0	7.9052E-08	3.0	2.2426E-02	2.8	8.3263E-08	2.8
1.50E-02	3.0433E-02	2.5	1.1687E-07	2.5	3.1626E-02	2.4	1.2353E-07	2.4
3.18E-02	8.9460E-02	1.6	5.9822E-07	1.6	1.0112E-01	1.5	6.7618E-07	1.5
8.65E-02	3.0754E-02	2.7	4.1333E-07	2.7	3.4242E-02	2.6	4.6021E-07	2.6
1.50E-01	2.5998E-02	2.6	6.4319E-07	2.6	3.1714E-02	2.3	7.8461E-07	2.3
2.24E-01	1.5619E-02	3.3	5.8916E-07	3.3	1.7134E-02	3.1	6.4626E-07	3.1
3.34E-01	1.4464E-02	3.4	7.8223E-07	3.4	1.5507E-02	3.0	8.3860E-07	3.0
4.98E-01	6.2744E-03	4.8	4.7071E-07	4.8	2.9261E-03	6.1	2.2674E-07	6.1
7.43E-01	3.8498E-03	6.3	3.9422E-07	6.3	1.0398E-03	9.9	1.0647E-07	9.9
9.07E-01	1.9980E-04	1.2	2.3796E-08	1.2	7.6687E-05	1.7	9.1334E-09	1.7
1.11E+00	1.1997E-04	1.5	1.5572E-08	1.5	4.7492E-05	2.1	6.1644E-09	2.1
1.35E+00	3.2361E-06	5.1	4.2101E-10	5.1	1.3447E-06	7.1	1.7494E-10	7.1
1.65E+00	6.3894E-07	10.5	8.2231E-11	10.5	5.7309E-07	11.6	7.3757E-11	11.6
2.02E+00	4.7331E-07	13.5	6.2205E-11	13.5	5.5083E-07	11.7	7.0065E-11	11.7
TOTAL	3.3745E-01	1.5	4.5356E-06	1.8	3.6433E-01	1.4	4.3877E-06	1.6